JOURNAL OF PROPULSION AND POWER
Vol. 15, No. 4, July–August 1999

Interferometric Study of Unsteady Passing Shock Flow in a Turbine Cascade

A. Wesner*
Johns Hopkins University, Applied Physics Laboratory, Laurel, Maryland 27023
and
J. A. Schetz† and H. Grabowski‡
Virginia Polytechnic Institute and State University, Blacksburg, Virginia 24061-0203

To further advance the state of the art in axial turbomachinery, a better understanding of unsteady phenomena within transonic turbines (including potential flow interaction, wake passing, and shock-wave passing) is required. Recently, the transonic turbine cascade facility at Virginia Polytechnic Institute and State University was modified to allow the study of unsteady passing shock flow. The steady interferometric system in place was updated to allow for a time-resolved, quantitative study of the density field produced by a single shock passing event. Variations in both the cascade inflow and flow through the transonic blade passages were quantized during the shock passage. The full density field in the cascade is presented at six discrete time intervals. A significant rise in the flow density, both upstream and on the suction side of the blade passage, was noted.

Nomenclature

f_{AB_f} = number of fringes between A and B, with flow
f_{AB_n} = number of fringes between A and B, no flow
K = constant, see Eq. (2)
L = test section span
λ = wavelength
ρ = density

Introduction

THE optimization of the aerodynamic and thermal performance of turbomachinery blading requires a detailed knowledge of the internal flowfield with respect to the factors that induce losses and promote heat transfer to the blade surface. These factors include boundary-layer growth, boundary-layer transition location, trailing-edge shock characteristics, and mixing losses downstream of the trailing edge. The flowfields encountered in current turbomachines are not only viscous and compressible, but also highly unsteady.[1,2] A better understanding of these unsteady phenomena is crucial for further improvements to advance the state of the art in axial turbomachinery. It has been widely documented that these flows have a significant influence on the efficiency, reliability, aeroelastic stability, forced response, and noise generation in modern axial-flow turbines.

Flow unsteadiness in turbine engines arises largely from the relative motion of the blade rows in the alternately stationary and rotating turbine stages. There are three major sources of flow unsteadiness in the interaction between turbine rotor and stator blade rows. The first cause of flow unsteadiness is a purely subsonic effect termed "potential flow interaction,"[3] where the complete inviscid flowfield around each blade is affected by the presence of the neighboring upstream and downstream blade rows. The second cause of flow unsteadiness in rotating turbine stages is termed "wake-passing." The wake-passing effect is caused by the repeated passage of a downstream blade row through the wakes shed from the trailing edges of the upstream stationary blade row. Of the three major sources of flow unsteadiness, potential flow interaction and wake effects have received considerable prior attention.

Third, for transonic turbines, significant unsteadiness occurs because of the nozzle guide vane (NGV) trailing-edge shock structure impinging on the downstream rotor blades.[4] This source of flow unsteadiness, shock-wave passing, has received much less attention because of the complexity of creating repeatable passing shock events at the required spacing to simulate a real engine environment. However, if progress is to be made in modern turbine blade design, reliable experimental results and computational methods will be required in this flow regime.

Recently, the transonic turbine cascade facility at Virginia Polytechnic Institute and State University (Virginia Tech) has been modified to allow the study of unsteady passing shock flow. Here, a shock tube is used to pass a two-dimensional shock along the cascade leading edge to simulate the shock impingement from a nozzle guide vane row onto the first high-pressure rotor stage in a transonic turbine engine. To allow for a quantitative, time-resolved study of this phenomena, we altered our previous steady interferometric flow visualization system.[5] The unsteady system design and initial results detailing the flowfield generated by a single passing shock are presented here.

To date, the most extensive research conducted on unsteady wake and shock passing was performed in the Isentropic Light Piston Tunnel of Oxford University.[6] In this facility, passing wakes and shocks are generated in a stationary cascade of highly loaded transonic turbine rotor blades by moving a row of wake-generating rods past the cascade at the required rotor velocity. The Oxford tunnel approximates ideal two-dimensional shocks and wakes over a single cascade passage by mounting the bars on the rim of a large-diameter rotating disk. Periodic shocks and wakes were produced by fitting the disk with a large number of bars, whereas only two bars on the disk gave isolated shock/wave events. Each rotating bar generates a bow shock wave, a wake, and a recompression shock wave. Another method of producing approximately two-dimensional shock/waves is the "squirrel cage" apparatus used by Pfeil et al.[7] and Bayley and Priddy.[8] The flow produced by both of these methods differs from the flow produced in an NGV, where the bow shock wave is absent.

Doorly and Oldfield[3] reported on the effects of passing shock waves and wakes on the heat transfer. Transient spikes in the blade

Presented as Paper 97-2751 at the AIAA/ASME/SAE/ASEE 33rd Joint Propulsion Conference, Seattle, WA, 6–9 July 1997; received 20 September 1997; revision received 10 July 1998; accepted for publication 29 July 1998.

*Research Associate, Research and Technology Development Center, M/S 10A-113, 11100 Johns Hopkins Road; awesner@aplcomm.jhuapl.edu. Member AIAA.

†J. Byron Maupin Professor, Aerospace and Ocean Engineering Department, 215 Randolph Hall; ptiger@vt.edu. Fellow AIAA.

‡Student, Aerospace and Ocean Engineering Department, 215 Randolph Hall; hgrabows@vt.edu. Student Member AIAA.

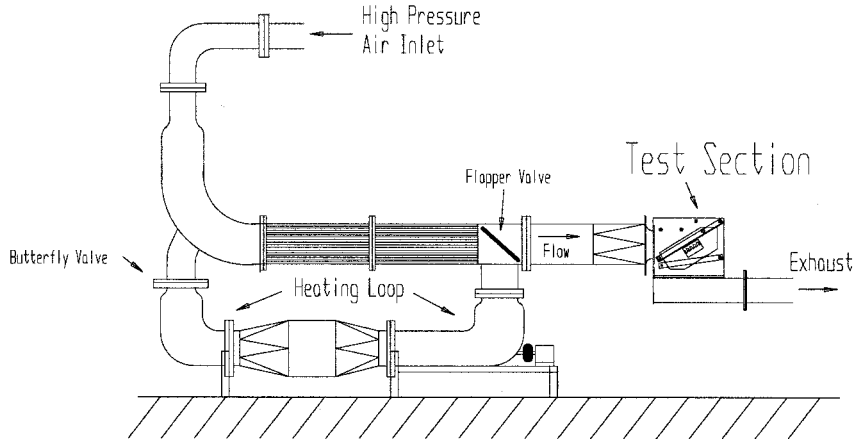

Fig. 1 Virginia Polytechnic Institute and State University Transonic Cascade Wind Tunnel.

suction surface heat transfer rate were found and attributed to the collapse of a leading-edge separation bubble. High-frequency shock wave impingements were found to have a complicated interaction and seemed to indicate that even relatively weak shock waves could have a noticeable effect on the boundary-layer transition process. These results were further supported by Schultz et al.[9] Detailed blade surface heat transfer rate measurements were made with high-response surface-resistance thermometers, enabling the wake and shock phenomena to be separated. It was found that the passage of the reduced velocity wake through the rotor blading gave rise to a time-varying change in incidence angle. This particularly affected the suction surface heat transfer rate and pressure distribution.

Johnson et al.[10] proposed an explanation different from the separation bubble proposed by Doorly and Oldfield[3] for the transient spikes in the surface heat transfer rate during the passing shock/wake event. Schlieren images and surface heat transfer measurements clearly detected the presence of a convecting bubble moving along the pressure surface, as opposed to the suction surface as seen in previous experimental results. The authors suggested that the feature was a vortical bubble formed at the blade leading edge from a shock-produced bifurcation.

All of the experimental work just described employed bars moving at high velocities along the leading edge of a linear cascade to produce combined passing shocks and wakes. Using this combination it is difficult to separate the effects caused solely by the passing shocks because of the unavoidable nonlinear interaction between the wake/shock events. Work recently conducted at Virginia Tech has concentrated exclusively on the unsteady effects produced by shock waves passing through transonic turbine rotor cascades to permit the study of the complex processes separately.

Experiments by Collie et al.[11] were the first to attempt developing a method to produce passing shock waves without wakes. Utilizing the explosion from a blank shotgun shell, the blast wave produced is shaped and directed through the cascade test section, parallel to the leading edge of the blade row. Using a specially designed shock shaper, highly repeatable single shocks could be produced, allowing data from numerous single shock events to be coupled. Spark shadowgraphs were used to track the propagation of the shock wave through the blade passage. The formation of the vortical bubble, described by Johnson et al.,[10] was also documented in the shadowgraphs. Other measurements centered around significant variations in the blade performance as the shock wave passed through the passage. A 120% peak-to-peak variation in estimated blade lift was found. Also, wake total pressure traverses found that the cascade loss coefficients fluctuated as much as 40% near the blade passage center because of shock-passing effects. Doughty and Schetz[12] abandoned the shotgun in favor of a shock tube. With this method, up to three variably spaced shocks can be directed into the cascade test section. This system for simulating the unsteady effects of shock waves is what is currently being used in the Virginia Polytechnic Institute and State University Transonic Cascade Wind Tunnel.

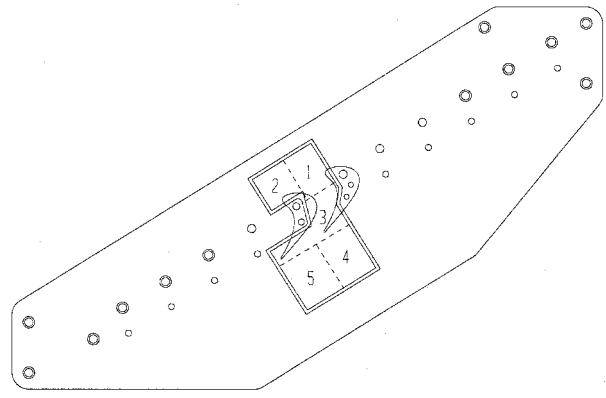

Fig. 2 Relative positioning of areas 1, 2, and 3 to the studied blade passage.

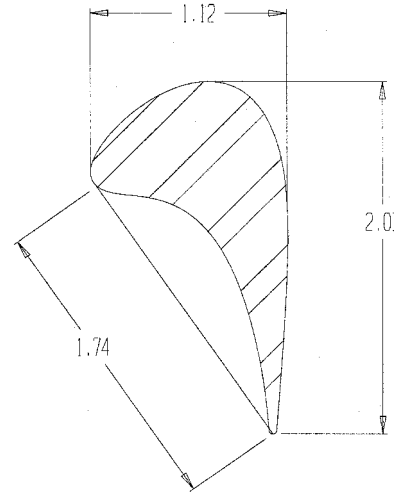

Fig. 3 Transonic turbine blade profile.

Facility

All of the experiments described here were conducted in the Virginia Polytechnic Institute and State University Transonic Cascade Wind Tunnel (Fig. 1). This facility is a blowdown-type cascade tunnel, providing up to 40 s of usable run time. The cascade consists of 11 turbine blades, two end blocks, and two aluminum endwalls fitted with precision crown glass inserts for optical access (Fig. 2). The cross section and dimensions of the blade studies are shown in Fig. 3. The blade was designed by General Electric and has a

3.81 cm (1.5 in.) axial chord and a 4.5 cm (1.77 in.) aerodynamic chord with an approximate turning angle of 127 deg. The span is 5.08 cm (2.0 in.) and the blades are spaced a distance of 3.81 cm (1.50 in.) apart. Labeling the 11 blades from the top of the cascade to the bottom (right to left), the blades of interest in this study are blades number 6 and number 7 (Fig. 2).

The shock-wave generation method developed for use in the transonic turbine cascade is a variation on the shock-tube system of Merritt and Aronson[13] (see Fig. 4). Utilizing a pressure-burst diaphragm shock tube, up to three shock waves are shaped and directed into the top of the transonic test section parallel to the leading-edge line of the blades. Three pressure-rated conduits extend from the end cap of the shock tube up to the top of the test section to create the three separate shocks. A diaphragm thickness of 24 mils was used for all of the shock tests, requiring a driver pressure of 576 psig for diaphragm failure. Only single passing shock experiments were performed.

A shock shaper was designed to reduce reflected shocks and create a two-dimensional shock face at the studied blade passage. A series of shadowgraph and high-frequency pressure studies were performed to optimize the shaper position and design. The studies included benchtop experiments into stationary air, performed using simulated Plexiglas® endwalls to allow optical access from all directions, as well as in situ tests, both with and without flow. These shadowgraph and pressure studies show that the shock is, in fact, fairly two dimensional at the blade passage being studied. Also, reflected shocks, created from the sudden area expansion as each shock wave enters the test section, are shown to dissipate before reaching the blade passage of interest. Figure 5 illustrates the positioning of the shock shaper relative to the cascade and shows a representative shock positioned within the test section. The nominal pressure rise upstream of the cascade generated by the initial shock passage is ~7.0% of the upstream static pressure. The shadowgraph and static pressure studies have also shown the shock locations and strengths to be repeatable to within ±10 ns and ±1.0 psi, respectively.[12]

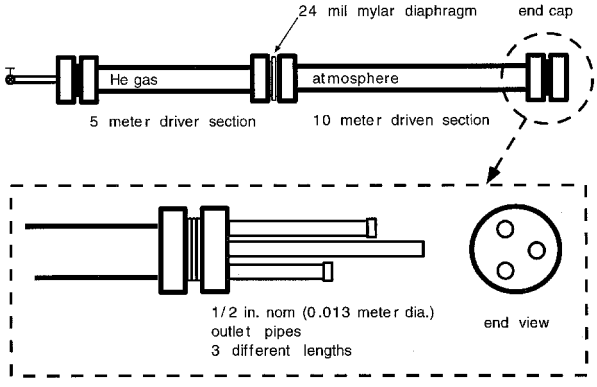

Fig. 4 Shock-tube construction.

Instrumentation

Interferometer

An optical interferometer is an instrument designed to exploit the interference of light and the fringe patterns that result from optical path differences. To achieve interference between two coherent beams of light, an interferometer divides an initial beam of light into two or more parts that travel different optical paths and then reunite to form an interference pattern.

The most commonly used type of interferometer is the Mach–Zehnder type (see Holder et al.[14] and Lightman and Cartwright[15] for a general discussion of these instruments). Because the light source used in a Mach–Zehnder-type interferometer is not coherent, it is necessary to adjust the path length difference between the reference and working beams to be less than one-tenth of a wavelength of the light, or 5×10^{-6} cm. Thus, this type of interferometer is very sensitive to temperature changes and mechanical vibrations.

The development of the laser introduced a source of highly coherent light, permitting the interference of wavefronts that propagated along various axes. The inherent improvement in coherence length relaxed the requirement for nearly identical path lengths between the arms of interferometric systems. The 1.0 in. (2.54 cm) path length difference created by the wedge plate in a single-plate interferometer was well within the allowable parameters. Figure 6 shows the basic optical components of a single-plate interferometric system. The wedge plate splits the light beam into two overlapping beams with a slight angle between them. It is the action of the wedge plate that causes fringe formation. The wedge plate is also the cause of the most distinct feature of single-plate interferograms, the presence of a double image. Because of the light reflection off both the front and rear surfaces of the wedge plate, all objects in the test section create two separate images at the image plane. The distance between the two images is referred to as the image separation distance. The second parabolic mirror is used to focus the parallel light beams. This image can be focused onto a photographic plate or a charge-coupled device (CCD) camera.

Several of the advantages of a single-plate interferometer over the Mach–Zehnder interferometer can now be seen. First, because the parallel beam is split only after it passes through the test section, no compensation chamber is needed. Also, because the wedge angle is fixed, there is no need for heavy vibration-free mounting of the wedge plate. Furthermore, only a single wedge plate is needed, compared with the two beam splitters and two flat mirrors required for the Mach–Zehnder interferometer. Finally, and most importantly, the setup of a single-plate system is simpler. Disadvantages include lower fringe quality and more difficult data interpretation. For a

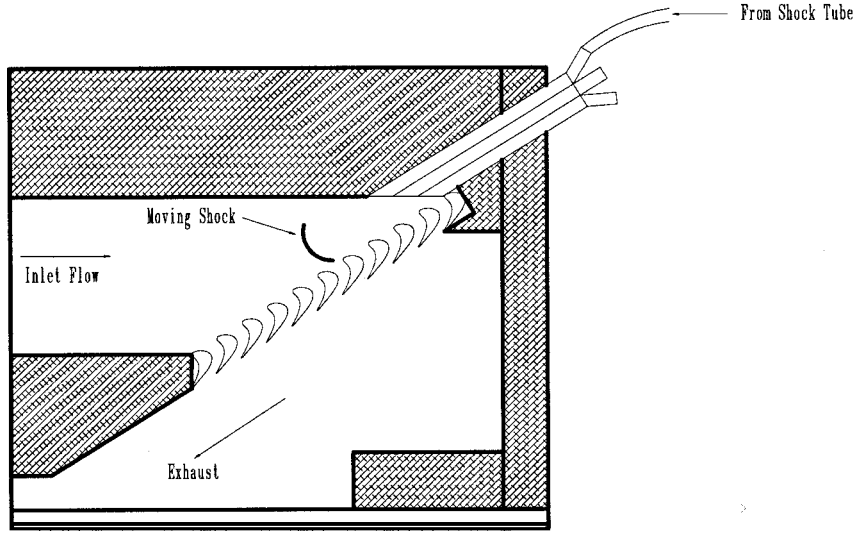

Fig. 5 Passing shock orientation within the test section.

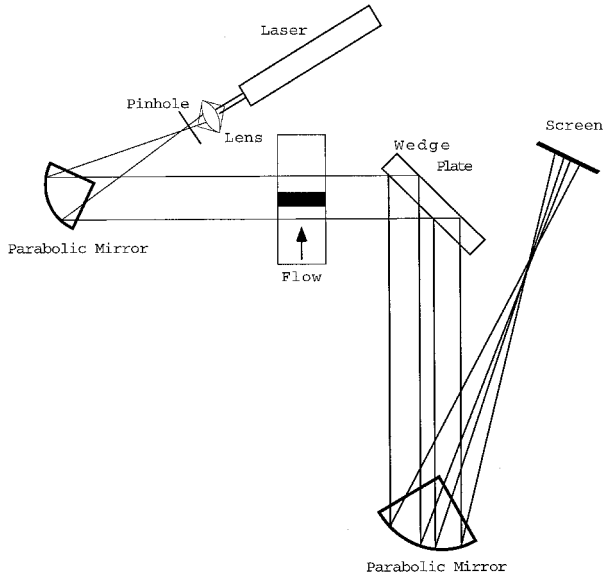

Fig. 6 Basic single-plate interferometric system.

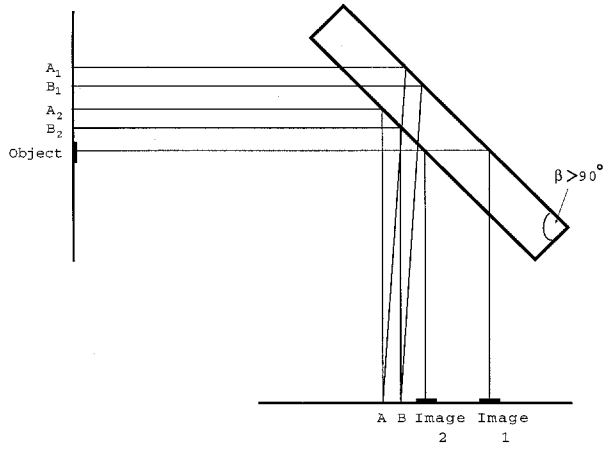

Fig. 7 Light path through single path.

single-plate interferogram, a domain in the flowfield with a known density distribution will be required; however, this flowfield can be chosen in a region where data acquisition is relatively easy. Details of interpreting single-plate interferograms can be found in the dissertation of Kiss.[5]

Figure 7 depicts the image formation for a certain orientation of the wedge plate. If one picks two points, A and B, in the interferogram, the A_1, A_2, B_1, and B_2 points can be traced back to the test section. Then, the following relationship can be written between the densities at these points:

$$\left(\rho_{A_1} - \rho_{B_1}\right) - \left(\rho_{A_2} - \rho_{B_2}\right) = -(\lambda_0/K)\left(f_{AB_f} - f_{AB_n}\right) \qquad (1)$$

The K constant is given by

$$K = \frac{Lk}{n_0 \rho_{\text{ref}}} \qquad (2)$$

where ρ_{ref} is the reference density of (1.252 kg/m^3) and $k = 3 \times 10^{-4}$.

Looking at Eq. (1), it is clear that if the absolute value of the density at a given point is to be found, the density must be known at three other locations. It can further be shown that when the density is known in a band having the width of the image separation distance d, the density can be found anywhere else in the studied flowfield. The two edges of the strip of width d will be two of the required known points, and the third will be from within the band. By moving across and down the band with the third known point, all of the densities in a new band of width d, located directly adjacent to the original band, can be calculated. This, in turn, is used to calculate a new band of known densities.

Some of the improvements to the existing steady system needed to produce viable unsteady interferograms are now described. In the unsteady flowfield of interest here, the passing shock generated by the shock tube travels through the test section at a nominal velocity of 340 m/s. The shock velocities of both the initial incident shock and all subsequent reflections are calculated using the temporal spacing of the voltage spikes from two closely spaced Kulite pressure transducers. The direction of shock travel was verified using a series of timed shadowgraphs. This flow feature is the driving force behind many of the required changes.

First of all, much shorter shutter times, of the order of 0.33 μs, are needed to capture the image of the passing shock without excessive blur. This shorter shutter time requires an increase in light intensity of at least two orders of magnitude at the photographic plane. Another problem is synchronizing the shuttering of the light source with the passing of the shock. Finally, the major problem of collecting a known density field in these unsteady conditions needed to be addressed as well as the difficulty of referencing all of the data together.

The first possibility investigated was simply switching to a pulsed laser system. Because of cost constraints, a high-powered pulsed laser system was prohibitively expensive. While researching various possibilities for increasing light intensity, a reference to intensified CCD cameras was uncovered. CCD intensifier cameras typically have nanosecond shuttering times and high gain capabilities. The addition of the CCD camera offered many advantages and simplifications.

To produce a sequence of timed interferograms showing the passing of the shock, a triggering and synchronizing mechanism was sought. While performing preliminary testing on the shock system, a simple setup using a high-frequency pressure transducer was employed to initiate the data collection. A high-frequency static pressure transducer is placed slightly upstream of the blade passage to be studied. As the shock passes, it creates a sharp pressure spike. This sharp pressure spike, with the addition of a time-delay circuit, triggers the shuttering of the CCD camera.

To produce the required known density field over a simple region of the flow, a variety of measurements needed to be performed. Factors in selecting the proper instrumentation included optical accessibility, flowfield disturbances, survivability, and frequency response. Because of these factors, it was decided to use a miniature hot wire specially constructed for use in the cascade's narrow blade passages to calculate the temperature changes of the flow as the shock wave passed upstream of the blades. These signals can also be synchronized off the spike on the upstream pressure transducer. Because the total pressure, static pressure, and total temperature were known prior to the initial passage of the shock, the pressure measurements could be used to calculate shock strengths, and, subsequently, the small total temperature and pressure variations caused by the passage of the initial incident shock and all subsequent reflections. The known static pressures and the small calculated total pressure variations were then used to calculate the flow velocities. Finally, using the flow velocities and total temperatures, the hot-wire data allowed calculation of the flow temperature and density.

Data Reduction

Because of the large number of images to be reduced, we elected to automate the fringe detection. Two C^{++} codes were written to reduce the gray-scale images to density values. The preprocessing algorithm has four main functions: image stretching, low-pass filtering, adaptive binarization, and line thinning. The second code performs the fringe counting and outputs the final reduced density values.

Image Preprocessing

The 512 $\times$ 480 pixels in the CCD camera are arranged in a square grid, thus the aspect ratio of each pixel is not the 1:1 aspect ratio required by the data reduction program. Therefore, a stretching

algorithm was employed to expand the distorted horizontal axis approximately by a factor of 1.21. This algorithm consists of two nested loops that traverse the destination image area pixel-by-pixel. For each pixel in the destination image, a reverse mapping is used to determine the corresponding pixel in the source image. Often this pixel address is a fractional value. This means that the calculated address would have fractional components of the neighboring pixels. Here, an interpolation technique is used. The four pixels that surround the calculated position of the destination pixel in the source image are fetched and a linear interpolation is used on pixel intensities to determine the destination pixel's gray-scale intensity value.

To reduce the presence of artifacts in the image introduced by the CCD camera and the frame grabber, it was necessary to spatially filter the image. A low-pass filter was used, taking great care in setting the upper frequency limit, to remove these artifacts without destroying any fringe details.

The image information output from a CCD camera is in a format known as gray scale. In this case, the CCD camera returns an eight-bit gray-scale image, providing 256 levels of gray. The image-processing techniques already employed required gray-scale images for proper processing. However, to detect the fringe edges and to enhance fringes that are lost in uneven background lighting, adaptive binarization (also referred to as adaptive thresholding) must be employed. In fixed thresholding, a single gray level is set as the cutoff level. Any pixel values falling under this level are set to 0 (black). Otherwise, the pixel value is set to 1 (white), producing a simple black and white image. Setting a single threshold level for the interferometric images is difficult because the image is disturbed by uneven lighting. Thus, a threshold level that adapts itself to the local gray-scale level is required. Locally adaptive binarization methods compute a threshold level for each pixel in the image on the basis of the information contained in the neighborhood of that pixel. The method employed here uses the idea of a threshold surface. If a pixel (x, y) in the input image has a higher gray level than the threshold surface evaluated at (x, y), then the pixel is labeled as background, otherwise it is labeled as an object (black). Our threshold surface consists of a 20×20 pixel block surrounding the studied pixel (x, y). The average gray level is computed in the 20×20 threshold surface and set as the threshold level for the surface.[16] Figure 8 shows an example of an adaptively binarized image. Because the binarization algorithm can leave extremely thick fringes that could complicate the fringe counting, it was necessary to process the binarized images with a line-thinning algorithm. The Hilditch algorithm was chosen for its robust nature and ease of implementation.[17] Figure 9 shows an example of a thinned image.

Uncertainty Analysis

A detailed uncertainty analysis was undertaken and can be found in the dissertation of Wesner.[18] Using the uncertainty values presented in the preceding text and values representative of typical data (without a shock directly over the reference domain) as jitter program inputs, an overall uncertainty value was found for the computed densities. By approximating the effects of the interpolation on the uncertainties of the reference pressure values, a simplified analytical analysis was performed. The values from both calculations compared favorably, lending validity to the jitter program formulation. The computed density value and overall uncertainty given by the jitter program was 2.808 ± 0.093 ($\pm 3.31\%$) kg/m^3.

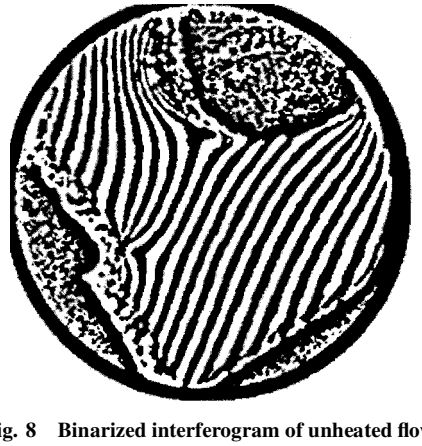

Fig. 8 Binarized interferogram of unheated flow.

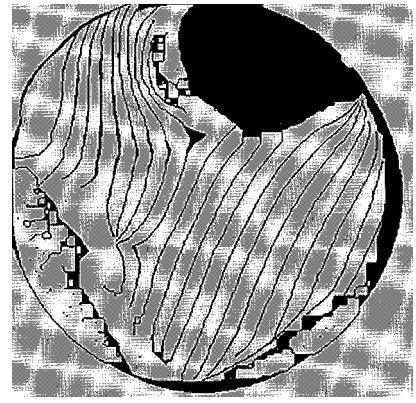

Fig. 9 Thinned interferogram of unheated flow.

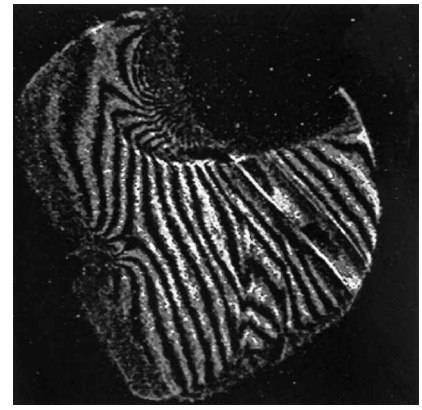

Fig. 10 Unsteady interferogram, 258 μs delay.

Results

Figure 10 shows the unsteady raw interferogram in area 1 of the cascade at a delay time of 256 μs after the initial shock passage. The raw single-plate interferometric images are difficult to visually interpret because they are flipped both horizontally and vertically as a result of optical manipulation of the light path. The bottom right of the image is upstream of the cascade and the upper left is in the blade passage. The initial shock wave travels from left to right across the bottom of the image. The characteristic double image of single-plate interferograms is easily seen by examining the turbine blade found in the upper right corner of the image. To reduce the interferograms, both a no-flow (an interferogram taken without any tunnel flow) and a flow image must be captured. In a no-flow interferogram, the density is constant; therefore, the fringes are nominally straight lines. When the cascade flowfield is generated and a flow image captured, the density variations shift the fringes. Any shock waves present in the flowfield are characterized by the coalescence of a large number of fringe lines, as can be seen on the right-hand side of Fig. 10. The raw data are converted to a density field using the procedure outlined previously. The reduced density field plots are presented next. First, the steady data will be introduced, and then the unsteady density field results will be discussed.

Figure 11 shows the density field results for the steady, adiabatic case. Portions of the blade are also shown for reference. As expected, the flow away from the cascade, toward the inlet, is fairly uniform with a density value ranging from between 2.4 and 2.5 kg/m^3. Also, the decrease in density as the flow enters the blade passage corresponds to the increase in velocity experienced by the flow as it is accelerated toward sonic velocity at the throat. Both the freestream

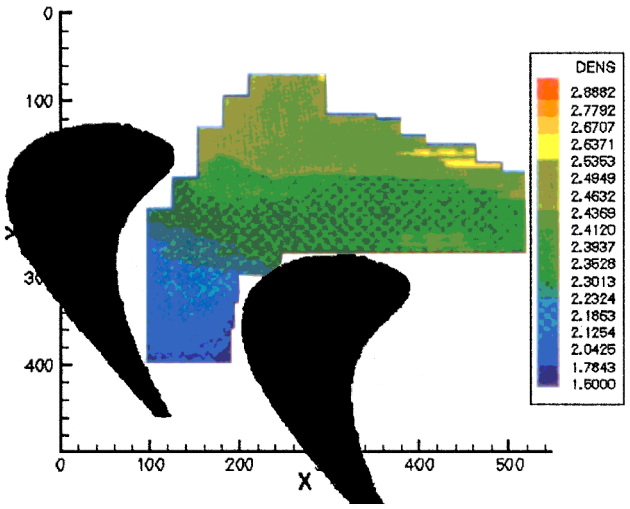

Fig. 11 Density field for adiabatic flow.

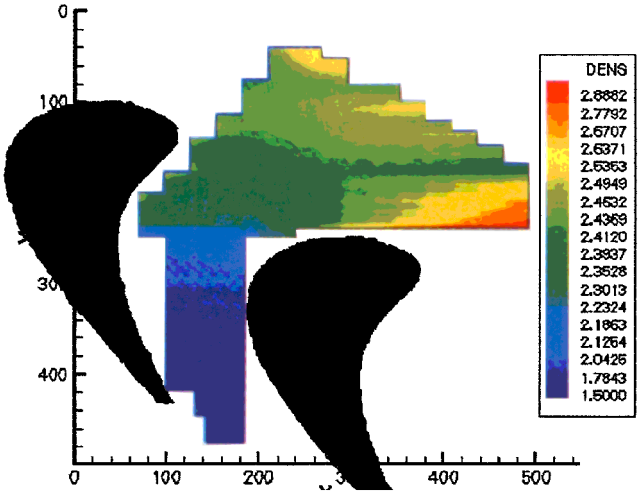

Fig. 12 Density field for 178 μs delay.

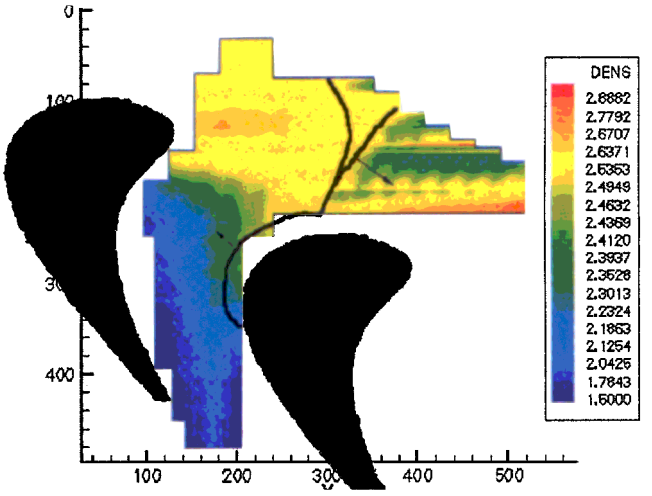

Fig. 13 Density field for 258 μs delay.

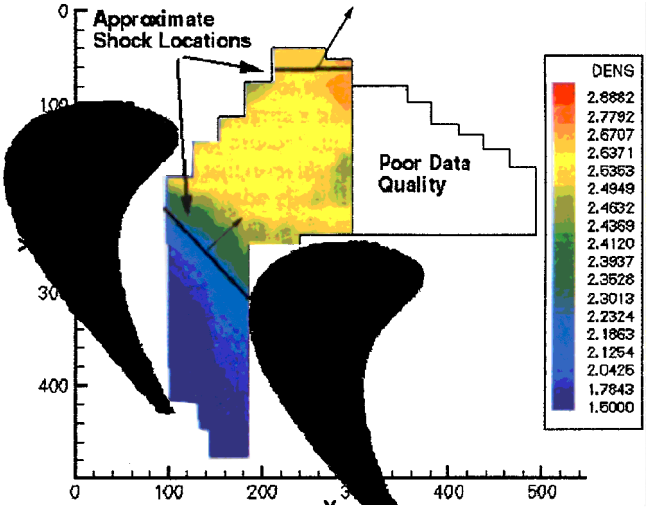

Fig. 14 Density field for 337 μs delay.

density values and those near the throat agree with values computed using a converging/diverging nozzle theory. Another feature of note is the increased density values near the leading edge of the blade in the left-hand lower corner of the plot where the flow is slowed by the presence of the blade. The extremely dark region in the lower corner is where the edge of the CCD image was encountered.

Now the unsteady results will be presented. The first density field is given at a delay time of 178 μs (Fig. 12). This is just prior to the entry into the studied domain; therefore, the flowfield is generally undisturbed. It should be noted, however, that even though a shock is normally associated with supersonic events, the passing shock is propagating into a subsonic flow; therefore, it can influence the upstream flowfield. Again, the same general flow features as found in the steady cases are found, although less pronounced.

In Fig. 13, taken at a delay time of 258 μs, the presence of the shock is clearly seen. In all of the density results, the approximate location of the shock is shown by a black line with arrows indicating the direction of travel. These shock locations were taken from a time-resolved shadowgraph study of the single shock passing event. The density behind the shock has increased to over 2.7 kg/m^3. The reflection from the suction surface of the lower blade of the initial shock is also shown. The passage of the reflection appears to have reduced the flow acceleration in the blade passage near the suction side, as evidenced by the elevated densities in this region.

As the shock moves farther upstream, the reflection generated as it passed over the blade propagates upstream and is moving out of the studied area by the time of the next interferogram (Fig. 14), taken at a delay time of 337 μs. Again, the presence of the shock wave is clearly visible in the density field. The density upstream of the blades is beginning to drop to more normal levels. Also, the initial suction surface reflection has reflected again off of the opposing pressure surface and is in the middle of the blade passage. The density around the suction surface of the lower blade is low around most of the blade although it does begin to recover some velocity from the initial shock passage through the throat. The poor quality of the data (not plotted here) was a result of poor fringe quality at the interface of the two image areas (area 1 and area 2, see Fig. 2).

At a delay time of 393 μs, the shock found in the blade passage at 337 μs has traveled upstream and again elevated the upstream densities (Fig. 15). The flow also shows an increase in density around the leading edge of the lower blade. Also, the presence of a complex shock pattern within the blade passage is again reducing the flow acceleration (especially near the suction side of the passage) caused by the converging section of the passage.

By a delay time of 465 μs, reflected shocks are still present within the passage, as seen in Fig. 16. However, both the upstream and passage flowfields appear to be recovering.

By a delay time of 518 μs, any reflected shock waves should be extremely weak. The overall density level upstream of the cascade remains elevated (Fig. 17). The passage of another reflection through the blade passage has again increased the density values near the blade suction surface. However, it is expected that if interferograms were taken at much longer delay times, the elevated levels would drop down near the undisturbed value. The flowfield appears to be

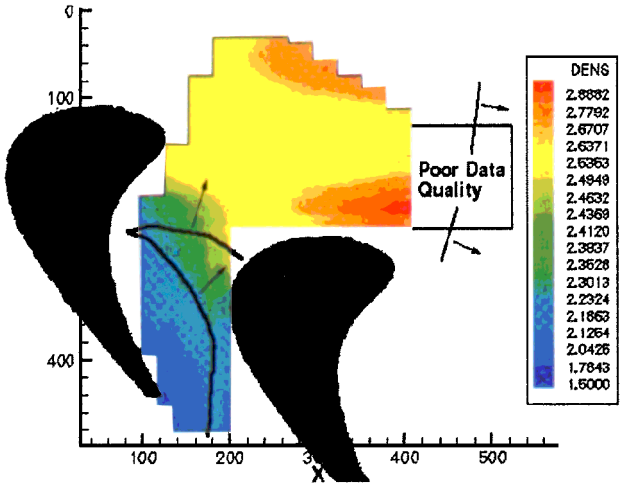

Fig. 15 Density field for 393 μs delay.

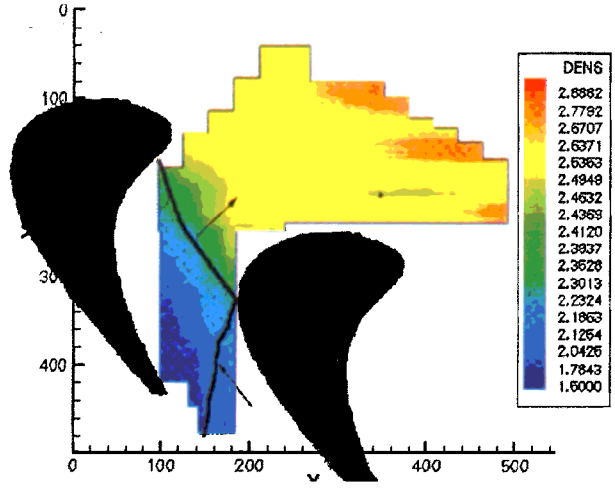

Fig. 16 Density field for 465 μs delay.

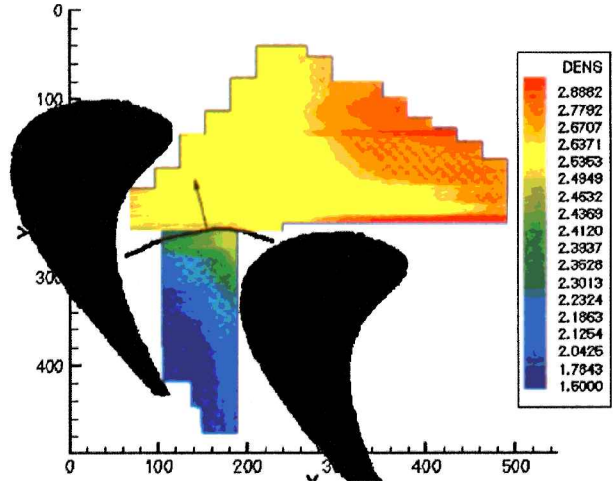

Fig. 17 Density field for 518 μs delay.

taking on the general features associated with the undisturbed flow, with a slight flow acceleration into the blade passage and slightly changed density values far upstream of the cascade.

Conclusions

A single-plate interferometric system capable of capturing unsteady passing shock events was successfully developed. This system incorporated advanced CCD technology to facilitate the freezing of a highly unsteady event, in this case that of a passing shock. Using this newly developed system, a study of the time history of the density field in a transonic turbine blade passage during a passing shock event was performed. The variations in the cascade inflow could be seen, not only during the initial shock passage, but during all of the subsequent reflections. A previous attempt made at performing an idealized analytical study of the passing shock event could only be performed up to the initial shock passing because of the large number variables in the system.[12] These measurements uniquely quantify this event and are a significant step in increasing our understanding of unsteady rotor/stator interactions with transonic turbine engines.

Optical methods hold a great advantage over traditional measurement systems in that there is little or no disturbance to the flowfield. Also, the entire flowfield can be studied simultaneously without having to resort to tedious pointwise measurement techniques. These factors are especially critical given the transonic flow conditions and small physical dimensions of the blades of interest here.

In the case of a single-plate interferometric system, the disadvantage of requiring a portion of the density field to be known and the difficulties inherent in the data reduction must be weighed against the simplicity of the setup. However, the area where the known reference density field is taken can be chosen to minimize the flow disturbances and increase the accuracy of the measurement.

The single-plate system did indeed prove simple to set up, a very important consideration when using shared facilities. The entire system setup could easily be performed in less than 2 h, compared with the days a Mach–Zehnder interferometer often requires. The replacement of the Polaroid film with the CCD camera proved advantageous. The internal shuttering mechanism of the CCD camera, removed the Bragg cell from the previous optical system, greatly reducing the effort required in the interferometric system setup. Also, because of the extremely quick shutter times used while working with the intensified CCD camera, it was no longer necessary to capture the images in a darkened room. This made the task of operating the tunnel simpler.

Using a combination of high-frequency pressure transducers and custom hot-wire probes, the required unsteady known density field was successfully recorded. To not disturb the flow in the blade passage, it was chosen to take the reference area upstream of the blade row. Timed shadowgraphs were used to choose shutter times where the shock wave was not situated within the studied density field to improve the accuracy of the results. One problem that was encountered was the passage of diaphragm fragments from the shock tube upstream of the test section after the passage of the shock. These diaphragm fragments had a tendency to break the hot wire. Because these fragments traveled behind the passing shock wave, the shock event was completed before the hot-wire lost continuity. However, because the number of required runs was high, the wire had to be replaced numerous times.

The newly developed unsteady interferometric system was tested under both steady and unsteady conditions. During steady operations, the experimentally obtained density field behaved as expected, decreasing in value as the flow entered the blade passage (corresponding to flow acceleration within the passage). Also, experimentally obtained densities showed excellent agreement to the calculated values, both upstream and near the nozzle throat. The reduced density field plots demonstrated the capability of the system to track the passage of the shock wave and the numerous reflections in a simulation of a NGV and high-pressure turbine rotor unsteady interaction. The expected pressure rise following the shock passage was shown in the density fields, and the effect of the passing shock on the inlet flow was clearly seen. Elevated densities were also seen near the blade suction surface following the passage of the incident shock and its reflection. This could be indicative of a reduction in the flow acceleration produced over the upper (suction) surface of the cascade during unsteady operation.

Areas for future work include the expansion of the study to evaluate the effect of multiple passing shock events. This would allow the quantitative study of the effect shock spacing (in time) has on the inlet flow and pressure rise of the density field, and also, on computational studies using the interferometric study for code validation. Databases generated with interferometric studies are crucial

in the development and improvement of computational fluid dynamic (CFD) codes. If CFD calculations are to be performed on this flowfield, it will be necessary to determine if the passing shock changes, temporally, the state of the boundary layer. And, finally, the improvement of the image-processing algorithms will allow the technique to be implemented more efficiently.

References

[1]Fottner, L., "Review on Turbomachinery Blading Design Problems," Lecture Series AGARD-LS-167, AGARD, May 1989.

[2]Janakiraman, S. V., "Fluid Flow and Heat Transfer in Transonic Turbine Cascades," M.S. Thesis, Mechanical Engineering Dept., Virginia Polytechnic Inst. and State Univ., Blacksburg, VA, May 1993.

[3]Doorly, D. J., and Oldfield, M. L. G., "Simulation of the Effects of Shock Wave Passing on a Turbine Rotor Blade," *Journal of Engineering for Gas Turbines and Power*, Vol. 107, Oct. 1985, pp. 998–1006.

[4]Rao, K. V., Delaney, R. A., and Dunn, M. G., "Vane-Blade Interaction in a Transonic Turbine, Part 1: Aerodynamics," *Journal of Propulsion and Power*, Vol. 10, No. 3, 1994, pp. 305–311.

[5]Kiss, T., "Experimental and Numerical Investigation of Transonic Turbine Cascade Flow," Ph.D. Dissertation, Mechanical Engineering Dept., Virginia Polytechnic Inst. and State Univ., Blacksburg, VA, Dec. 1992.

[6]Doorly, D. J., and Oldfield, M. L. G., "Simulation of Wake Passing in a Stationary Turbine Rotor Cascade," *Journal of Propulsion and Power*, Vol. 1, No. 4, 1985, pp. 316–318.

[7]Pfeil, H., Herbst, R., and Schröder, T., "Investigation of the Laminar-Turbulent Transition of Boundary Layers Disturbed by Wakes," *Journal of Turbomachinery*, Vol. 105, No. 2, 1983, pp. 130–137.

[8]Bayley, F. J., and Priddy, W. J., "Effects of Free-Stream Turbulence on the Distribution of Heat Transfer Around Turbine Blade Sections," *International Journal of Heat Fluid Flow*, Vol. 6, No. 3, 1985, pp. 181–191.

[9]Schultz, D. L., Johnson, A. B., Ashworth, D. A., Rigby, M. J., and LaGraff, J. E., "Wake and Shock Interactions in a Transonic Turbine Stage," *AGARD 68th Specialists' Meeting, Transonic and Supersonic Phenomena in Turbomachines*, No. 3, 1986, pp. 1–16.

[10]Johnson, A. B., Oldfield, M. L. G., Rigby, M. J., and Giles, M. B., "Nozzle Guide Vane Shock Wave Propagation and Bifurcation in a Transonic Turbine Cascade," ASME 35th Int. Gas Turbine and Aeroengine Congress and Exposition, American Society of Mechanical Engineers, TR 90-GT-310, June 1990.

[11]Collie, J. C., Moses, H. L., Schetz, J. A., and Gregory, B. A., "Recent Advances in Simulating Unsteady Flow Phenomena Brought About by Passage of Shock Waves in a Linear Turbine Cascade," *Journal of Turbomachinery*, Vol. 115, Oct. 1993, pp. 687–698.

[12]Doughty, R. L., and Schetz, J. A., "Cascade Simulation of Multiple Shock Passing from Upstream Blade Rows," *Loss Mechanisms and Unsteady Flows in Turbomachines*, Neuilly sur Seine, France, 1996.

[13]Merritt, D. L., and Aronson, P. M., "Study of Blast-Bow Wave Interactions in a Wind Tunnel," AIAA Paper 65-5, March 1965.

[14]Holder, D. W., North, R. J., and Wood, G. P., "Optical Methods for Examining the Flow in High-Speed Wind Tunnels," AGARD, Ottawa, Canada, Nov. 1956.

[15]Lightman, A. J., and Cartwright, S., "Techniques for Optical Interferanemography," U.S. Air Force Wright Aeronautical Labs., AFWAL-TR-85-3098, Dec. 1985.

[16]Trier, Ø. D., and Taxt, T., "Evaluation of Binarization Methods for Document Images," *IEEE Transaction on Pattern Analysis and Machine Intelligence*, Vol. 17, March 1995, pp. 312–315.

[17]Bush, L. J., "Evaluating the Accuracy of Line Thinning Algorithms After Processing Scanned Line Data," M.S. Thesis, Electrical Engineering Dept., Virginia Polytechnic Inst. and State Univ., Blacksburg, VA, 1993.

[18]Wesner, A. L., "An Interferometric Study of Unsteady Passing Shock Flow in a Turbine Cascade," Ph.D. Dissertation, Aerospace and Ocean Engineering Dept., Virginia Polytechnic Inst. and State Univ., Blacksburg, VA, Oct. 1996.

Color reproductions courtesy of Johns Hopkins University, Applied Physics Laboratory and Virginia Polytechnic Institute and State University.